RSC Advances

PAPER

View Article Online
View Journal | View Issue

Cite this: *RSC Adv.*, 2023, **13**, 212

The eight structures of caffeic acid: a jet-cooled laser ablated rotational study†

G. Juárez, M. Sanz-Novo, R. Aguado, J. L. Alonso, I. León * and E. R. Alonso *

Received 9th November 2022
Accepted 4th December 2022

DOI: 10.1039/d2ra07124j

rsc.li/rsc-advances

This work reports a complete conformational analysis of caffeic acid, an exceptionally versatile pharmacophore, using laser ablation chirped-pulse Fourier transform microwave spectroscopy. The whole conformational space consisting of eight distinct species has been fully deciphered based on the trend of the rotational constants supported by theoretical computations. We show how rotational spectroscopy can be confidently used to distinguish between conformers even when the structural differences are minimal, such as those involved in the conformational panorama of caffeic acid. Additionally, the structural information here provided, such as the planarity observed in all the conformers, could help to elucidate the mechanisms underlying the biological and pharmacological activity of hydroxycinnamic acids.

Introduction

In recent decades, natural products have been portrayed as essential scaffolds in drug design and discovery.[1] Despite a myriad of small organic and biomolecules employed in the search for potential therapeutical agents, phenolic acids stand above the rest.[2–5] This family of compounds is widespread in nature, with over 50 000 diverse species identified so far,[6,7] and can be classified into different groups according to their molecular structure.[8] Among them, of paramount importance are hydroxycinnamic acids, which are present in nearly all plants.[9–11] The principal representative hydroxycinnamic acid is caffeic acid (*trans*-3-(3,4-dihydroxy phenyl)prop-2-enoic acid), commonly found in food as several simple derivatives such as esters and amides.[12,13] The pharmacological profile of this molecule and its derivatives is quite broad, highlighting their potential use as anti-cancerigenous[14–17] and anti-inflammatory agents,[18–20] as well as manifesting a remarkable antioxidant and scavenging activity.[21–24] It is well known that the aforementioned biomedical properties mainly rely on the corresponding structure–activity relationship.[25] Hence, deciphering the shape of these species at the molecular scale is crucial to better understand the mechanisms underlying their biological activity.

What can we expect from the conformational panorama of caffeic acid? Based on purely chemical intuition, we can anticipate a conformational landscape consisting of eight distinct structures due to four different torsional degrees (see Fig. 1). In this context, several experimental investigations have been devoted to studying this archetypal hydroxycinnamic acid using IR, NMR, UV, terahertz, and X-ray diffraction techniques.[26–28] Surprisingly, the prior experimental scenario delineated a somewhat simple conformational panorama of only one configuration.[26] Note that these studies are limited to condensed phases, where intermolecular interactions with the surrounding media might alter or even restrict conformational behavior. Thus, a thorough investigation under the isolation conditions of the gas phase is mandatory to provide compelling information on the intrinsic conformational behavior of caffeic acid.

High-resolution microwave spectroscopy is a spectroscopic technique capable of facing this challenging problem. Rotational spectroscopy is extremely sensitive to the molecular geometry so that conformers of caffeic acid can be discerned as totally different species, and the assignments rely on the consistency of many rotational lines measured for each conformer. One unique aspect of rotational studies is that even very subtle changes in the molecular structure are translated into a distinctive array of spectroscopic constants.[29–31] Nevertheless, the major constraint of transferring caffeic acid to the gas phase is its solid nature (mp 213 °C) and its inherent vaporization problems. Nowadays, it has become possible to explore the architecture of solid biomolecules in the gas phase by techniques that couple laser ablation (LA), for transferring them intact into the gas phase, with high-resolution Fourier transform microwave (FTMW) techniques in a supersonic

Grupo de Espectroscopía Molecular (GEM), Edificio Quifima, Laboratorios de Espectroscopía y Bioespectroscopía, Unidad Asociada CSIC, Parque Científico Uva Universidad de Valladolid, Paseo de Belén 5, 47011 Valladolid, Spain. E-mail: elenarita.alonso@uva.es

† Electronic supplementary information (ESI) available: In Section 1 we provide the original LA-CP-FTMW broadband spectrum of caffeic acid (Fig. S1). We collect in Section 2 a complete list of the measured frequencies and residuals (in MHz) for all the observed rotamers of caffeic acid (see Tables S1–S8). Finally, in Section 3 we display the Cartesian coordinates of the caffeic acid conformers optimized at B3LYP-GD3BJ/6-311++G(d, p), which are shown in Tables S9–S16. See DOI: https://doi.org/10.1039/d2ra07124j

expansion. The low-temperature environment of a supersonic expansion provides the ideal medium for preparing individual conformers of caffeic acid in virtual isolation conditions, ready to be interrogated by a short burst of microwave radiation. The Fourier transformation of the temporal profile of the emerging radiation yields rotational spectra of unprecedented resolution and sensitivity. These combined techniques have been established as an exceptionally robust tool to investigate the conformational landscape of many solid biomolecules[31–35] and, particularly, systems showing intricate conformational panoramas.[35–40] This experimental approach has been recently extended to the related *trans*-cinnamic and *trans-p*-coumaric phenolic acids.[41]

In this work, we have examined the gas phase structure of caffeic acid using our broadband LA-CP-FTMW technique.[33,42] As we will see below, comparing the experimental spectroscopic constants with those predicted theoretically enables us to conclusively identify the conformers of caffeic acid. These findings are of interest to unveil the role of caffeic acid as a versatile pharmacophore and lead the search for more effective caffeic acid derivatives.

Experimental methods

Caffeic acid was obtained commercially and used without further purification. The sample was pulverized and mixed with a small amount of commercial binder, which was needed to provide enough consistency to the rod. Then it was pressed into a cylindrical die to obtain a rod, which was vaporized by the third harmonic (355 nm) of a Nd:YAG picosecond laser. We use a motor controller, which allows a DC motor to rotate and translate the rod up and down along the injection system to achieve homogeneous exploitation of the solid rod. The ablation products, seeded in a flow of neon at a stagnation pressure of 12 bar, were supersonically expanded and characterized by chirped pulse Fourier transform microwave spectroscopy. Details of the instrumental setup working from 2–8 GHz have been reported elsewhere.[43,44] In this experiment, chirped pulses of 4 μs directly generated by the 24 GS s^{-1} arbitrary waveform generator (Tektronix AWG7122B), were amplified to about 300 W peak power using a traveling wave tube amplifier (IFI, GT186-300). The amplified pulse was broadcasted through microwave horn antennas inside the vacuum chamber, perpendicularly intercepting the pulsed-jet expansion. At a repetition rate of 2 Hz, a total of 62 000 free induction decays (4 FID emissions per gas pulse), each with a 10 μs length, were averaged and digitized using a 50 GS s^{-1} digital oscilloscope. The frequency-domain spectrum in the 2.75–6.50 GHz frequency range (see Fig. S1a†) was obtained by taking a fast Fourier transform (FFT) following the application of a Kaiser–Bessel window to improve the baseline resolution. We usually attain line widths (full-width-half-maximum, FWHM) of approximately 100 kHz due to the perpendicular direction of the sample injection with respect to the microwave field, which is further translated in a relatively short transit time of the polarized molecular jet. Frequency measurements were extended up to 14 GHz (see Fig. S1b†) using a parabolic reflector system described in detail elsewhere.[42,45] We estimate the uncertainty of the line measurements in both configurations to be better than 20 kHz.

Results and discussion

Theoretical modelling

Prior to the experimental work, we extended the previous DFT calculations on the conformational space of caffeic acid[46] and performed additional computations to predict molecular conformational properties relevant to the investigation of the rotational spectrum. The method of choice was the hybrid density functional B3LYP, including the Grimme dispersion[47,48] with Becke–Johnson damping.[49,50] As anticipated, the complete conformational panorama consists of eight distinct conformations (see Fig. 1) of remarkable stability, all lying below 400 cm^{-1}. They are therefore expected to be observed in the supersonic jet. Table 1 provides rotational constants and electric dipole moment components to guide the spectral searches and assignments.

The candidate structures can be sorted into two *syn* and *anti* families according to the different orientations of the pendant ring with respect to the *meta*-OH group (see Fig. 1). As seen in Table 1, this event gives rise to a specific and substantial change in their moments of inertia, which is further transferred into the rotational constants. For each family, four different conformers arise from a variation in the disposition of the terminal carboxyl group (*cis* or *trans*) or a change in the orientation of the catechol hydroxyl group (clockwise, *a*, and counterclockwise, *b*). As shown in Table 1, the values of rotational constants are extremely close within each family because of their similar mass distribution. We can thus anticipate that the analysis of the rotational spectrum will be a difficult task.

Broadband LA-CP-FTMW rotational spectrum

We recorded the broadband spectrum of caffeic acid in the 2.75–6.50 GHz range using our laser ablation chirped-pulse Fourier transform microwave (LA-CP-FTMW) spectrometer.[33,42] As usually in our LA experiments,[51] we first removed instrumental artifacts and photo-fragmentation lines from the spectra, including those familiar to the previous study on *trans*-cinnamic and *trans-p*-coumaric acids.[41] The resulting spectrum, shown in Fig. 2A, appears highly dense due to the anticipated noticeable number of rotameric species of caffeic acid. At first glance, guided by our theoretical computations, we identified strong progressions dominating the spectrum. They were ascribed to *b*-type R-branch transitions from a first rotamer I (✶). We extended the assignment to *b*-type *Q*-branches and weaker *a*-type R-branch lines. The corresponding rigid rotor analysis give rise to the experimental spectroscopic constants collected in the first column of Table 2. At first look, the experimental values of the rotational constants are consistent with those predicted for all the *syn*-family conformers. Rotamer I exhibits an intense *b*-type and a weak *a*-type rotational spectrum, according to the predicted values of the dipole moment components for *syn-cis-a* conformer in Table 1. Thus, it is

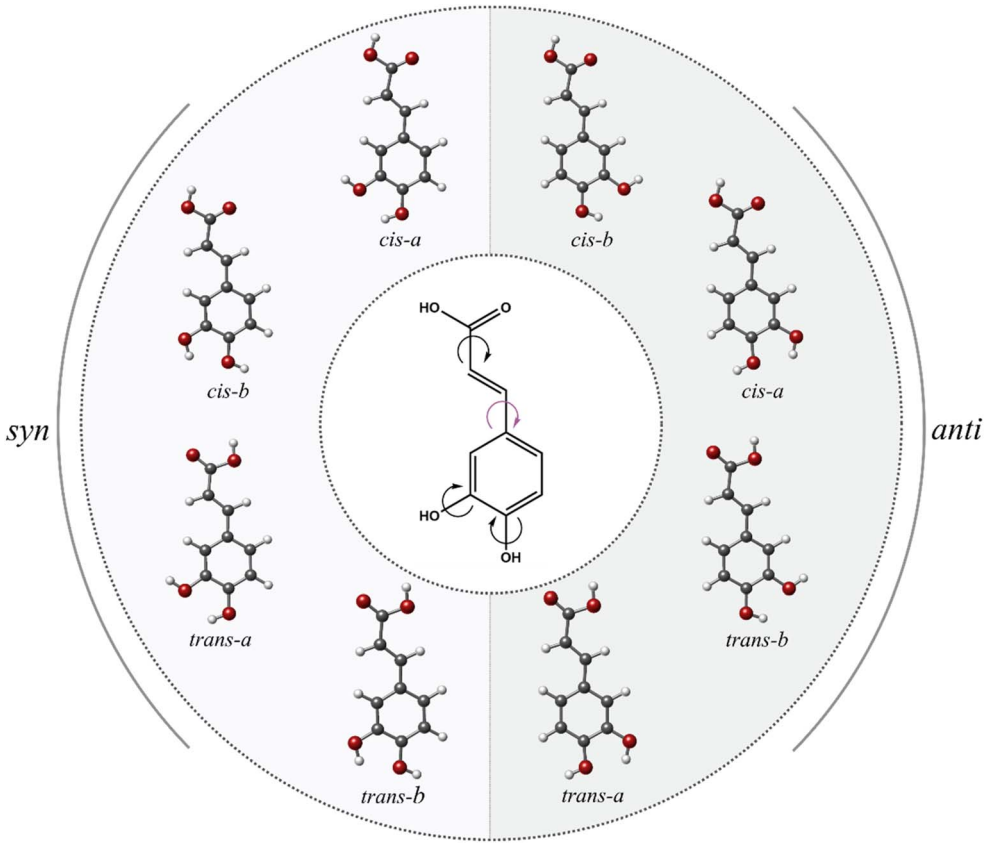

Fig. 1 The entire conformational space of caffeic acid.

Table 1 Calculated spectroscopic parameters for the caffeic acid conformers

	Syn-				*Anti-*			
Parameter	*Cis-a*	*Cis-b*	*Trans-a*	*Trans-b*	*Cis-b*	*Cis-a*	*Trans-b*	*Trans-a*
A^a	2269.4	2269.4	2279.1	2279.6	2479.6	2479.1	2463.5	2463.4
B	321.5	322.1	323.1	323.7	309.6	309.9	312.2	312.5
C	281.6	282.1	283.0	283.4	275.2	275.4	277.1	277.3
μ_a	1.7	4.2	2.1	4.6	2.0	3.3	2.8	4.2
μ_b	3.0	1.2	0.2	4.0	0.9	3.8	3.5	1.2
μ_c	0.0	0.0	0.0	0.0	0.0	0.0	0.0	0.0
$\Delta E_{ZPE}{}^b$	0	139	145	334	65	213	276	364
ΔG^c	0	161	133	336	44	135	223	364

[a] A, B, and C represent the rotational constants (in MHz); μ_a, μ_b and μ_c are the electric dipole moment components (in D). [b] Relative energies (in cm^{-1}) with respect to the global minimum, taking into account the zero point energy (ZPE). [c] Gibbs energies (in cm^{-1}) were calculated at 298 K. Theoretical computations were carried out at the B3LYP-GD3/6-311++G(d, p) level of theory.

reasonable to ascribe it to the global minimum *syn-cis-a* conformer as starting point.

Continuing the analysis, we found satellite lines around the transitions of rotamer I that may be attributable to other *syn*-conformers. We succeeded in assigning three *a*-type R-branch progressions to the other three rotamers belonging to the *syn* family; II (●), III (◆), and IV (⬣). The rotational constants derived from the corresponding rigid rotor analyses are also listed in Table 2, and the measured rotational transitions are collected in Tables S1–S4 of the ESI.†

At this point, we achieved a complete conformational identification based on a thorough investigation of the trend of the rotational constant's values comparing predicted and experimental changes (see Fig. 3). Hence, when going from rotamer I to rotamer II, the observed changes in the rotational constants are $\Delta A = 1.7$ MHz, $\Delta B = 0.6$ MHz, and $\Delta C = 0.5$ MHz, which perfectly match with the theoretically predicted ones of $\Delta A = 0.0$ MHz, $\Delta B = 0.6$ MHz, and $\Delta C = 0.5$ MHz in going from *syn-cis-a* to *syn-cis-b* (see Fig. 3). It points to the identification of rotamer I as *syn-cis-a* and rotamer II as *syn-cis-b*, respectively.

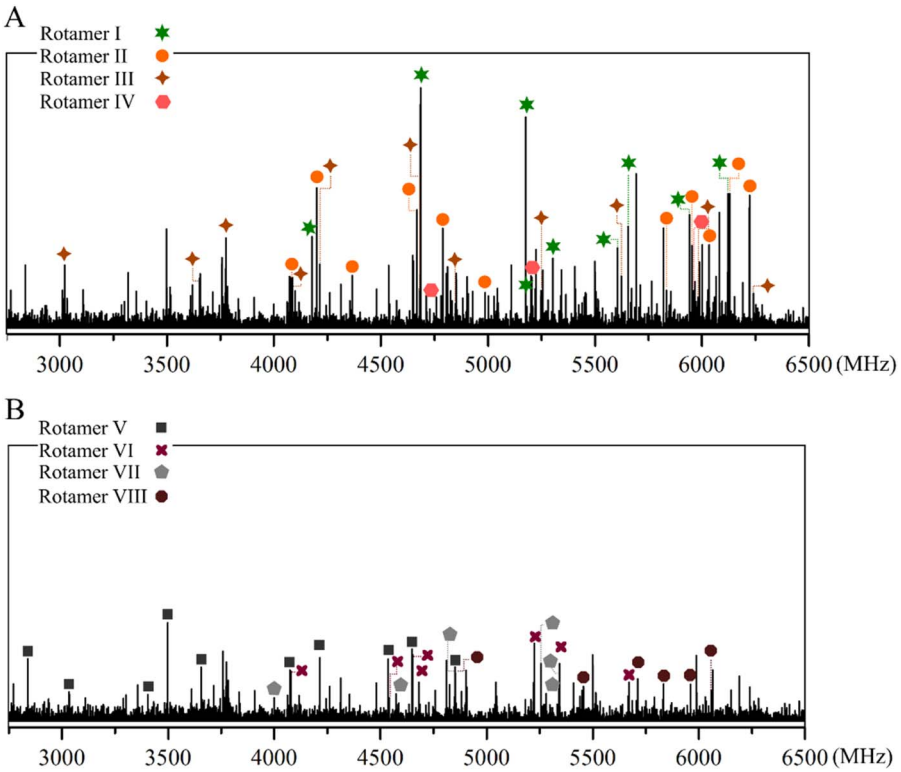

Fig. 2 (A) Broadband CP-FTMW rotational spectrum of caffeic acid from 2.75 to 6.50 GHz showing characteristic R-branch progressions for rotamers I–IV; (B) remaining spectrum resulting from removing the lines ascribable to rotamers I–IV. Transitions belonging to rotamers V–VIII are depicted. Intensity is given in arbitrary units.

Table 2 Experimental spectroscopic parameters for the caffeic acid rotamers I–IV

	Rotamer I	Rotamer II	Rotamer III	Rotamer IV
A^a	2262.22348 (78)[e]	2263.95 (20)	2271.20 (49)	2272.9750 (10)
B	321.88280 (31)	322.45623 (55)	323.51160 (12)	324.00522 (45)
C	281.96625 (23)	282.4286 (54)	283.36153 (98)	283.77359 (41)
Δ^b	−1.1	−1.1	−1.2	−1.2
μ_a	Observed	Observed	Observed	Observed
μ_b	Observed	—	—	Observed
μ_c	—	—	—	—
σ^c	14.4	11.6	18.2	14.9
N^d	55	16	14	27

[a] A, B, and C represent the rotational constants (in MHz); μ_a, μ_b, and μ_c are the electric dipole moment components. [b] $\Delta = I_c - I_a - I_b$ in μÅ^2. Conversion factor: 505 379.07 μÅ^2 MHz. [c] Rms deviation of the fit (kHz). [d] Number of fitted transitions. [e] Standard error in parentheses in units of the last digit.

Fig. 3 shows that the predicted changes in rotational constants in going from the *syn-cis-b* to *syn-trans-a* conformer are in excellent agreement with those derived from the experimental values of Table 2 when going from rotamer II to rotamer III, thus leading again to the conclusion that rotamer II is *syn-cis-b*. The observed changes between rotamers III and IV are only consistent with those calculated for the *syn-trans-a* and *syn-trans-b* conformers. Furthermore the *b*-type R-branch transitions observed for rotamer IV have a similar intensity compared

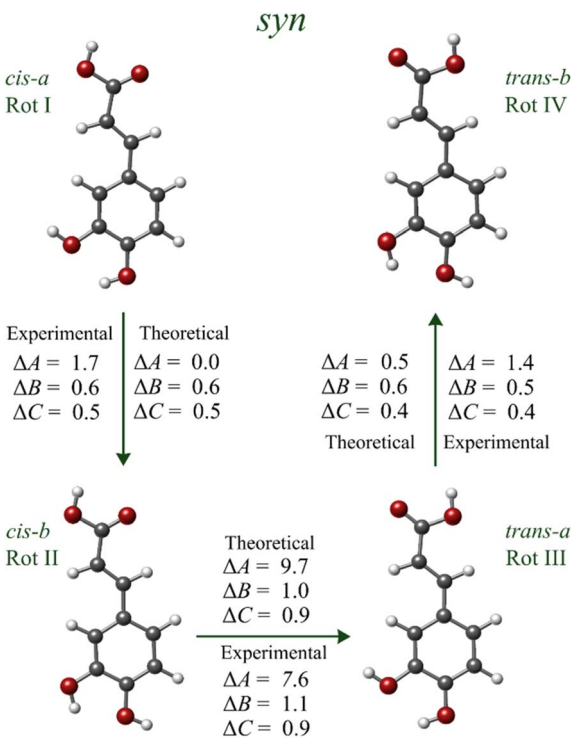

Fig. 3 Experimental and calculated changes in the values of the rotational constants for rotamers I–IV (in MHz).

to the *a*-type transitions, confirming that it belongs to the *syn-trans-b* conformer, which has a similar value for the predicted μ_a and μ_b dipole moments. Overall, the experimental compliance of the theoretical trend supports our identification and the consistency of the whole conformational assignment.

Once the four *syn* conformers were analyzed, we removed all their signals from the broadband spectrum, generating the spectrum of Fig. 2B, on which the identification of the *trans* family conformers was addressed. We employed the same strategy to the *anti*-conformers and identified a dominant *a*-type R-branch progression attributable to rotamer V (■), which was tentatively assigned to the *anti-cis-b* conformer based on the dipole moment selection rules and line intensities. Then, we searched for lines that fall in the proximity of those belonging to rotamer V and found new *a*-type progressions ascribable to the three VI (✚), VII (⬟), and VIII (●) rotamers. For rotamers VI and VII, *b*-type R-branch transitions were also observed. The experimental rotational constants derived from rigid rotor analysis are listed in Table 3, and the measured transitions are reported in Tables S5–S8 of the ESI.† The values of the rotational constants are consistent with those predicted for the *anti*-conformers in Table 1.

Once again, we need to inspect the trend of the rotational constant's values to decipher the subtle structural changes between each *anti*-conformer and attain a definite conformational identification. For the *anti*-family, these minimal differences (*i.e.*, the reorganization of the OH groups) produce once more very mild yet specific shifts in the rotational constants, which serve as conclusive proof to assign each structure while "travelling" between conformers (see Fig. 4). Therefore, once we have identified rotamer V as the *anti-cis-b* conformer, we can tie rotamers VI, VII, and VIII to conformers *anti-cis-a*, *anti-trans-b*, and *anti-trans-a*, respectively. The small experimental changes observed in the values of the rotational constants are again in harmony with the calculated shifts at the B3LYP-GD3/6-311++G(d, p) level of theory in Fig. 4, corroborating the conformational identification. Additionally, the dipole moment selection rules and intensities allow us to confirm further the identification of rotamer VI and VII as conformers *anti-cis-a* and *anti-trans-b*.

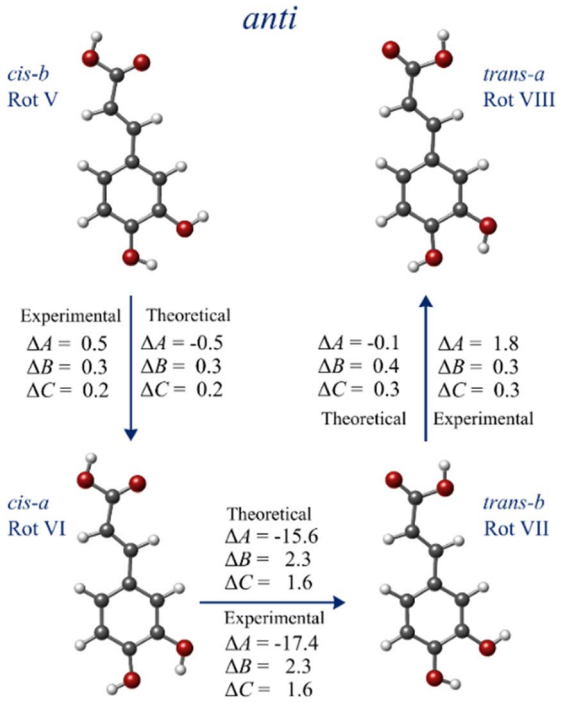

Fig. 4 Experimental and calculated changes in the values of the rotational constants for rotamers V–VIII (in MHz).

Table 3 Experimental spectroscopic parameters for the caffeic acid rotamers V–VIII

	Rotamer V	Rotamer VI	Rotamer VII	Rotamer VIII
A^a	2473.82 (67)[e]	2474.36056 (90)	2456.980 (13)	2458.81 (93)
B	309.7585 (85)	310.02508 (40)	312.2982 (48)	312.6236 (11)
C	275.4663 (83)	275.70948 (25)	277.28203 (49)	277.5706 (12)
Δ^b	−1.2	−1.4	−1.3	−1.4
μ_a	Observed	Observed	Observed	Observed
μ_b	—	Observed	Observed	—
μ_c	—	—	—	—
σ^c	13.9	14.3	15.4	16.1
N^d	14	40	22	7

[a] A, B, and C represent the rotational constants (in MHz); μ_a, μ_b and μ_c are the electric dipole moment components. [b] $\Delta = I_c - I_a - I_b$ in μÅ^2. Conversion factor: 505 379.07 μÅ^2 MHz. [c] Rms deviation of the fit (kHz). [d] Number of fitted transitions. [e] Standard error in parentheses in units of the last digit.

Although we tried to estimate the relative population of the detected conformers based on the intensity measurement of the rotational transitions and the predicted dipole moments, any quantitative information is meaningless as the number of fitted transitions for some of the less stable species is small. Nevertheless, we found that the experimental relative population, based on the spectral intensity produced by each detected conformer, follows the tendency given by the theoretical relative energies in Table 1. This is another point supporting that B3LYP-GD3/6-311++G(d, p) is a good choice for caffeic acid.

Regarding the structure–activity relationship of caffeic acid, it is known that some of the most important features of potent antioxidants consist on the presence of planar phenylopropanoic moieties stabilized by resonance (mainly in radical and radical cation forms) as well as catechol hydroxyl groups (OH groups attached to a benzene ring). Moreover, they can be reinforced by the presence of additional electron donating functional groups such as hydroxyl and methoxyl groups.[52] The eight structures of caffeic acid exhibit small negative values of the inertial defect, varying between −1.4 and −1.1 μÅ^2, which implies that all are planar with C_s symmetries. The small negative values are due to the contribution of the out-of-plane C(ph)–C–C–COOH torsion to the inertial deffect.[53–56] Note that *c*-type transitions were not observed, in accordance with the $\mu_c = 0$ dipole moment component expected for planar structures. This structural feature, present in all the caffeic structures, highlight a deluge of possibilities for the caffeic acid scaffold to act as a pharmacophore.

Conclusions

The present study provides the first experimental information on naked caffeic acid. We have transferred the solid sample into the gas phase by laser ablation and probed it in the isolation conditions of a supersonic expansion by Fourier transform microwave spectroscopy. The spectroscopic data directly compared with those computated theoretically *in vacuo* constitutes an unmatched tool to achieve the unambiguous identification of the eight planar conformers of caffeic acid that constitute its conformational landscape. High-resolution rotational spectroscopy has allowed us to unveil subtle structural changes between each conformer. We are pushing the limits of rotational spectroscopy, highlighting its potential as an outstanding characterization technique for the investigation of very similar structures exhibiting analogous rotational constants, as in the case of caffeic acid.

The structural information provided in this work should be of interest to comprehend the physical–chemical properties shown by this archetypal hydroxycinnamic acid and shall ultimately shed light on the mechanisms underlying its biological and pharmacological activity. Additionally, our investigation may help as a preliminary step in designing new caffeic acid-based pharmacophores.

We have proven once more the superb potential of rotational spectroscopy on the structural study of relevant biomolecules. Within this framework, we plan to extend our research to unveil the shape of more natural products that have remained, until now, elusive for high-resolution rotational studies.

Conflicts of interest

The authors declare no competing financial interests.

Acknowledgements

The financial funding from Ministerio de Ciencia e Innovación (PID2019-111396GB-I00), and Junta de Castilla y León (VA244P20) is acknowledged. G. J. acknowledges funding from the Spanish "Ministerio de Ciencia, Innovación y Universidades" under the predoctoral FPI Grant (BES-2017-082173).

References

1 N. Kumar and N. Goel, Phenolic Acids: Natural Versatile Molecules With Promising Therapeutic Applications, *Biotechnol. Rep.*, 2019, **24**, e00370.
2 M. Touaibia, J. Jean-Francois and J. Doiron, Caffeic Acid, A Versatile Pharmacophore: An Overview, *Mini-Rev. Med. Chem.*, 2012, **11**, 695–713.
3 G. G. Gross, *Biosynthesis And Metabolism Of Phenolic Acids And Monolignols*, Academic Press, Inc., 1985.
4 C. Clé, L. M. Hill, R. Niggeweg, C. R. Martin, Y. Guisez, E. Prinsen and M. A. K. Jansen, Modulation Of Chlorogenic Acid Biosynthesis In Solanum Lycopersicum; Consequences For Phenolic Accumulation And UV-Tolerance, *Phytochemistry*, 2008, **69**, 2149–2156.
5 H. Ravn, C. Andary, G. Kovács and P. Mølgaard, Caffeic Acid Esters As *In Vitro* Inhibitors Of Plant Pathogenic Bacteria And Fungi, *Biochem. Syst. Ecol.*, 1989, **17**, 175–184.
6 J. Ávila-Román, J. R. Soliz-Rueda, F. I. Bravo, G. Aragonès, M. Suárez, A. Arola-Arnal, M. Mulero, M. J. Salvadó, L. Arola, C. Torres-Fuentes and B. Muguerza, Phenolic Compounds And Biological Rhythms: Who Takes The Lead?, *Trends Food Sci. Technol.*, 2021, **113**, 77–85.
7 A. M. Boudet, Evolution And Current Status Of Research In Phenolic Compounds, *Phytochemistry*, 2007, **68**, 2722–2735.
8 R. Dixon, Natural Products And Plant Disease Resistance, *Nature*, 2001, **411**, 1–5.
9 M. N. Clifford, Chlorogenic Acids And Other Cinnamates - Nature, Occurrence And Dietary Burden, *J. Sci. Food Agric.*, 1999, **79**, 362–372.
10 L. Li, P. R. Shewry and J. L. Ward, Phenolic Acids In Wheat Varieties In The Healthgrain Diversity Screen, *J. Agric. Food Chem.*, 2008, **56**, 9732–9739.
11 L. Nyström, M. Mäkinen, A. M. Lampi and V. Piironen, Antioxidant Activity Of Steryl Ferulate Extracts From Rye And Wheat Bran, *J. Agric. Food Chem.*, 2005, **53**, 2503–2510.
12 V. L. Singleton, J. Zaya and E. K. Trousdale, Caftaric And Coutaric Acids In Fruit Of Vitis, *Phytochemistry*, 1986, **25**, 2127–2133.
13 M. N. Clifford, Chlorogenic Acids And Other Cinnamates - Nature, Occurrence, Dietary Burden, Absorption And Metabolism, *J. Sci. Food Agric.*, 2000, **80**, 1033–1043.
14 P. Michaluart, J. L. Masferrer, A. M. Carothers, K. Subbaramaiah, B. S. Zweifel, C. Koboldt, J. R. Mestre, D. Grunberger, P. G. Sacks, T. Tanabe and A. J. Dannenberg, Inhibitory Effects Of Caffeic Acid Phenethyl Ester On The Activity And Expression Of Cyclooxygenase-2 In Human Oral Epithelial Cells And In A Rat Model Of Inflammation, *Cancer Res.*, 1999, **59**, 2347–2352.
15 W. Y. Huang, Y. Z. Cai and Y. Zhang, Natural Phenolic Compounds From Medicinal Herbs And Dietary Plants: Potential Use For Cancer Prevention, *Nutr. Cancer*, 2010, **62**, 1–20.
16 J. L. Slavin, Mechanisms For The Impact Of Whole Grain Foods On Cancer Risk, *J. Am. Coll. Nutr.*, 2000, **19**, 300S–307S.
17 S. Mirzaei, M. H. Gholami, A. Zabolian, H. Saleki, M. V. Farahani, S. Hamzehlou, F. B. Far, S. O. Sharifzadeh, S. Samarghandian, H. Khan, A. R. Aref, M. Ashrafizadeh, A. Zarrabi and G. Sethi, Caffeic Acid And Its Derivatives As Potential Modulators Of Oncogenic Molecular Pathways: New Hope In The Fight Against Cancer, *Pharmacol. Res.*, 2021, **171**, 105759.
18 P. C. Chao, C. C. Hsu and M. C. Yin, Anti-Inflammatory And Anti Coagulatory Activities Of Caffeic Acid And Ellagic Acid In Cardiac Tissue Of Diabetic Mice, *Nutr. Metab.*, 2009, **6**, 1–8.
19 H. Kırmızıbekmez, Y. İnan, R. Reis, H. Sipahi, A. C. Gören and E. Yeşilada, Phenolic Compounds From The Aerial Parts of Clematis Viticella L. And Their *In Vitro* Anti-Inflammatory Activities, *Nat. Prod. Res.*, 2019, **33**, 2541–2544.

20 F. Paciello, A. Di Pino, R. Rolesi, D. Troiani, G. Paludetti, C. Grassi and A. R. Fetoni, Anti-Oxidant And Anti-Inflammatory Effects Of Caffeic Acid: *In Vivo* Evidences In A Model Of Noise-Induced Hearing Loss, *Food Chem. Toxicol.*, 2020, **143**, 111555.

21 I. Gülçin, Antioxidant Activity Of Caffeic Acid (3,4-dihydroxycinnamic acid), *Toxicology*, 2006, **217**, 213–220.

22 O. M. Agunloye, G. Oboh, A. O. Ademiluyi, A. O. Ademosun, A. A. Akindahunsi, A. A. Oyagbemi, T. O. Omobowale, T. O. Ajibade and A. A. Adedapo, Cardio-Protective And Antioxidant Properties Of Caffeic Acid And Chlorogenic Acid: Mechanistic Role Of Angiotensin Converting Enzyme, Cholinesterase And Arginase Activities In Cyclosporine Induced Hypertensive Rats, *Biomed. Pharmacother.*, 2019, **109**, 450–458.

23 M. Spiegel, A. Gamian and Z. Sroka, A Statistically Supported Antioxidant Activity DFT Benchmark—The Effects Of Hartree–Fock Exchange And Basis Set Selection On Accuracy And Resources Uptake, *Molecules*, 2021, **26**, 5058.

24 B. Veeren, M. Bringart, C. Turpin, P. Rondeau, C. Planesse, I. Ait-Arsa, F. Gimié, C. Marodon, O. Meilhac, M. P. Gonthier, N. Diotel and J. L. Bascands, Caffeic Acid, One Of The Major Phenolic Acids Of The Medicinal Plant Antirhea Borbonica, Reduces Renal Tubulointerstitial Fibrosis, *Biomedicines*, 2021, **9**, 358.

25 J. C. Morales and R. Lucas, *Structure-Activity Relationship of Phenolic Antioxidants and Olive Components*, Elsevier Inc., 2010.

26 S. Garcia-Granda, G. Beurskens and P. T. Beurskens, Structure of 3, 4-Dihydroxy-*trans*-cinnamic Acid (Caffeic Acid) and Its Lack Of Solid-State, *Acta Crystallogr.*, 1987, **43**, 683–685.

27 R. Świsłocka, Spectroscopic (FT-IR, FT-Raman, UV absorption, 1H and 13C NMR) And Theoretical (In B3LYP/6-311++G** Level) Studies On Alkali Metal Salts Of Caffeic Acid, *Spectrochim. Acta, Part A*, 2013, **100**, 21–30.

28 T. Chen, Y. Huang, Z. Tang, D. Liang and X. Yin, Terahertz Spectral Vibrational Properties And Weak Interactions Analysis Of Caffeic Acid And Ferulic Acid, *J. Mol. Struct.*, 2022, **1270**, 133960.

29 J. L. Alonso, I. Peña, J. C. López and V. Vaquero, Rotational Spectral Signatures Of Four Tautomers Of Guanine, *Angew. Chem., Int. Ed.*, 2009, **48**, 6141–6143.

30 M. Sanz-Novo, M. Mato, I. León, A. M. Echavarren and J. L. Alonso, Shape-Shifting Molecules: Unveiling The Valence Tautomerism Phenomena In Bare Barbaralones, *Angew. Chem., Int. Ed.*, 2022, **61**, 1–6.

31 J. L. Alonso and J. C. López, in *Gas-Phase IR Spectroscopy and Structure of Biological Molecules*, Springer International Publishing, 2015, p. 335.

32 C. Cabezas, M. Varela and J. L. Alonso, The Structure Of The Elusive Simplest Dipeptide Gly-Gly, *Angew. Chem., Int. Ed.*, 2017, **56**, 6420–6425.

33 E. R. Alonso, I. León and J. L. Alonso, *The Role of The Intramolecular Interactions In The Structural Behavior Of Biomolecules: Insights From Rotational Spectroscopy*, Elsevier, 2021, pp. 93–141.

34 I. León, E. R. Alonso, S. Mata, C. Cabezas and J. L. Alonso, Unveiling The Neutral Forms Of Glutamine, *Angew. Chem., Int. Ed.*, 2019, **58**, 16002–16007.

35 I. León, M. Fusè, E. R. Alonso, S. Mata, G. Mancini, C. Puzzarini, J. L. Alonso and V. Barone, Unbiased Disentanglement Of Conformational Baths With The Help Of Microwave Spectroscopy, Quantum Chemistry, And Artificial Intelligence: The Puzzling Case Of Homocysteine, *J. Chem. Phys.*, 2022, **157**, 074107.

36 A. Simaõ, C. Cabezas, I. León, E. R. Alonso, S. Mata and J. L. Alonso, Elucidating The Multiple Structures Of Pipecolic Acid By Rotational Spectroscopy, *Phys. Chem. Chem. Phys.*, 2019, **21**, 4155–4161.

37 E. R. Alonso, I. León, L. Kolesniková, S. Mata and J. L. Alonso, Unveiling Five Naked Structures Of Tartaric Acid, *Angew. Chem., Int. Ed.*, 2021, **60**, 17410–17414.

38 G. T. Fraser, R. D. Suenram and C. L. Lugez, Investigation Of Conformationally Rich Molecules: Rotational Spectra Of Fifteen Conformational Isomers Of 1-Octene, *J. Phys. Chem. A*, 2001, **105**, 9859–9864.

39 S. R. Domingos, C. Pérez, C. Medcraft, P. Pinacho and M. Schnell, Flexibility Unleashed In Acyclic Monoterpenes: Conformational Space Of Citronellal Revealed By Broadband Rotational Spectroscopy, *Phys. Chem. Chem. Phys.*, 2016, **18**, 16682–16689.

40 V. W. Y. Tsoi, E. Burevschi, S. Saxena and M. E. Sanz, Conformational Panorama of Cycloundecanone: A Rotational Spectroscopy Study, *J. Phys. Chem. A*, 2022, **126**, 6185–6193.

41 V. Cortijo, E. R. Alonso, S. Mata and J. L. Alonso, Conformational Map Of Phenolic Acids, *J. Phys. Chem. A*, 2018, **122**, 646–651.

42 E. R. Alonso, *Biomolecules and Interstellar Molecules: Structure, Interactions and Spectroscopic Characterization*, PhD thesis, Universidad de Valladolid, Spain, 2018.

43 S. Mata, I. Peña, C. Cabezas, J. C. López and J. L. Alonso, A Broadband Fourier-Transform Microwave Spectrometer With Laser Ablation Source: The Rotational Spectrum Of Nicotinic Acid, *J. Mol. Spectrosc.*, 2012, **280**, 91–96.

44 G. G. Brown, B. C. Dian, K. O. Douglass, S. M. Geyer and B. H. Pate, The Rotational Spectrum Of Epifluorohydrin Measured By Chirped-Pulse Fourier Transform Microwave Spectroscopy, *J. Mol. Spectrosc.*, 2006, **238**, 200–212.

45 I. Peña, S. Mata, A. Martín, C. Cabezas, A. M. Daly and J. L. Alonso, Conformations of D-Xylose: The Pivotal Role of the Intramolecular Hydrogen-Bonding, *Phys. Chem. Chem. Phys.*, 2013, **15**, 18243, and references therein.

46 E. VanBesiena and M. P. M. Marques, Ab Initio Conformational Study of Caffeic Acid, *J. Mol. Struct.: THEOCHEM*, 2003, **625**, 265–275.

47 A. D. Becke, A new mixing of Hartree–Fock and local density-functional theories, *J. Chem. Phys.*, 1993, **98**, 1372–1377.

48 S. Grimme, J. Antony, S. Ehrlich and H. Krieg, A Consistent And Accurate *Ab Initio* Parametrization Of Density Functional Dispersion Correction (DFT-D) For The 94 Elements H-Pu, *J. Chem. Phys.*, 2010, **132**, 154104.

49 S. Grimme, S. Ehrlich and L. Goerigk, Effect Of The Damping Function In Dispersion Corrected Density Functional Theory, *J. Comput. Chem.*, 2011, **32**, 1456–1465.
50 E. R. Johnson and A. D. Becke, A Post-Hartree-Fock Model Of Intermolecular Interactions: Inclusion Of Higher-Order Corrections, *J. Chem. Phys.*, 2006, **124**, 9.
51 L. Kolesniková, I. León, E. R. Alonso, S. Mata and J. L. Alonso, An Innovative Approach For The Generation Of Species Of The Interstellar Medium, *Angew. Chem.*, 2021, **133**, 24666–24671.
52 E. G. Bakalbassis, N. Nenadis and M. Tsimidou, A Density Functional Theory Study Of Structure-Activity Relationships In Caffeic And Dihydrocaffeic Acids And Related Monophenols, *JAOCS, J. Am. Oil Chem. Soc.*, 2003, **80**, 459–466.
53 T. Oka, On Negative Inertial Defect, *J. Mol. Struct.*, 1995, **352–353**, 225–233.
54 J. L. Alonso and R. M. Villamañan, Rotational Isomerism In Monofluorobenzaldehydes, *J. Chem. Soc.*, 1989, **85**, 137–149.
55 R. M. Villamañan, J. C. López and J. L. Alonso, On the Planarity of 2-Fluorostyrene, *J. Am. Chem. Soc.*, 1989, **111**, 6487–6491.
56 M. Sanz-Novo, E. R. Alonso, I. León and J. L. Alonso, The Shape Of The Archetypical Oxocarbon Squaric Acid And Its Water Clusters, *Chem.–Eur. J.*, 2019, **25**, 10748–10755.